


RESEARCH ARTICLE | MAY 22 2024

# Deep learning and random light structuring ensure robust free-space communications **FREE**

Xiaofei Li ; Yu Wang ; Xin Liu ; Yuan Ma ; Yangjian Cai  ; Sergey A. Ponomarenko  ; Xianlong Liu  

 Check for updates

*Appl. Phys. Lett.* 124, 214103 (2024)

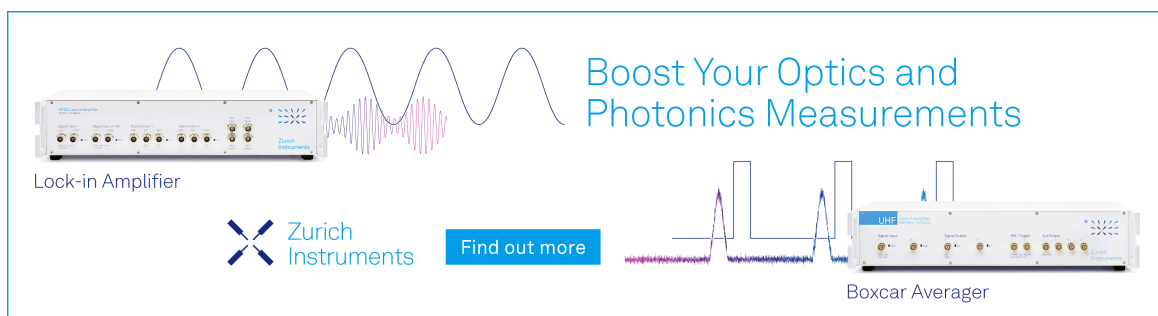
<https://doi.org/10.1063/5.0203326>



View Online




Export Citation



Boost Your Optics and Photonics Measurements

Lock-in Amplifier

 Zurich Instruments

[Find out more](#)

Boxcar Averager

# Deep learning and random light structuring ensure robust free-space communications

Cite as: Appl. Phys. Lett. **124**, 214103 (2024); doi: [10.1063/5.0203326](https://doi.org/10.1063/5.0203326)

Submitted: 15 March 2024 · Accepted: 13 May 2024 ·

Published Online: 22 May 2024



View Online



Export Citation



CrossMark

Xiaofei Li,<sup>1,2</sup> Yu Wang,<sup>3</sup> Xin Liu,<sup>1</sup> Yuan Ma,<sup>2</sup> Yangjian Cai,<sup>1,a)</sup> Sergey A. Ponomarenko,<sup>2,4,a)</sup> and Xianlong Liu,<sup>1,a)</sup>

## AFFILIATIONS

<sup>1</sup>Shandong Provincial Engineering and Technical Center of Light Manipulation and Shandong Provincial Key Laboratory of Optics and Photonic Devices, School of Physics and Electronics, Shandong Normal University, Jinan 250014, China

<sup>2</sup>Department of Electrical and Computer Engineering, Dalhousie University, Halifax, Nova Scotia B3J 2X4, Canada

<sup>3</sup>School of Information Science and Engineering, Shandong Normal University, Jinan 250014, China

<sup>4</sup>Department of Physics and Atmospheric Science, Dalhousie University, Halifax, Nova Scotia B3H 4R2, Canada

<sup>a)</sup>Authors to whom correspondence should be addressed: [yangjiancai@sndu.edu.cn](mailto:yangjiancai@sndu.edu.cn); [serpo@dal.ca](mailto:serpo@dal.ca); and [xianlongliu@sndu.edu.cn](mailto:xianlongliu@sndu.edu.cn)

## ABSTRACT

Having shown early promise, free-space optical (FSO) communications face formidable challenges in the age of information explosion. The ever-growing demand for greater channel communication capacity is one of the challenges. The inter-channel crosstalk, which severely degrades the quality of transmitted information, creates another roadblock in the way of efficient implementation of FSO communication systems. Here, we advance theoretically and realize experimentally a potentially high-capacity FSO protocol that enables high-fidelity transfer of an image or set of images through a complex environment. In our protocol, we complement random light structuring at the transmitter with a deep learning image classification platform at the receiver. Multiplexing unique, independent, mutually orthogonal degrees of freedom available to structured random light can potentially significantly boost the channel communication capacity of our protocol without introducing any deleterious crosstalk. Specifically, we show how one can multiplex the degrees of freedom associated with the source coherence radius and a spatial position of a beamlet within an array of structured random beams to greatly enhance the capacity of our communication link. The superb resilience of structured random light to environmental noise, as well as extreme efficiency of deep learning networks at classifying images, guarantees high-fidelity image transfer within the framework of our protocol.

Published under an exclusive license by AIP Publishing. <https://doi.org/10.1063/5.0203326>

In the age of information explosion, there has been growing demand for high-capacity communication systems due to relentless growth of traffic through any available communication channel.<sup>1</sup> To achieve high-capacity communications within the framework of free-space optics, it is essential that all available degrees of freedom of a light field be explored and engaged. To date, a number of approaches to boost the transmission capacity of free-space optical communications have been proposed,<sup>2–4</sup> including a quadrature phase shift keying,<sup>5</sup> wavelength division multiplexing,<sup>6</sup> space division multiplexing,<sup>7</sup> and polarization division multiplexing.<sup>8</sup> To further increase the channel capacity to overcome the existing bottlenecks, orbital angular momentum division multiplexing has recently been proposed.<sup>9–11</sup> Apart from capacity limitations, though, free-space optical communications are hampered by transmission quality degradation owing to data crosstalk.<sup>12</sup> The latter is chiefly due to the challenge posed by a realistic transmission medium involving atmospheric turbulence and/

or solid particles, such as aerosols, in the light path from a source (transmitter) to a receiver.<sup>10</sup> Indeed, the refractive index of the atmosphere fluctuates due to the temperature and humidity variations, giving rise to turbulent effects. The atmospheric fluctuations distort the phase of a transmitted light beam, causing deleterious crosstalk among multiple independent degrees of freedom (DoFs) of a free-space communication link.<sup>12</sup> As atmospheric turbulence seriously hinders further progress toward high-quality, high-capacity optical communications through a realistic complex environment, numerous strategies have been proposed to remedy the channel crosstalk.<sup>13–16</sup> In addition to multiple adaptive optics techniques, which can be subdivided into two main groups, pre-compensation and post-compensation,<sup>10</sup> there is a spatial polarization differential phase shift keying technology for vector light beams<sup>17</sup> and scattering-matrix-assisted retrieval protocol.<sup>18</sup> Unfortunately, virtually all these strategies require complicated, and often time-consuming, data processing and they invariably fail to lower

crosstalk to an acceptable level. Furthermore, to compensate for light scattering obstacles in the transmission path, self-healing coherent light sources, such as the ones generating Bessel beams, have been employed to help self-reconstruct transmitted image structure past opaque obstructions.<sup>19,20</sup>

At the same time, recent work has established extraordinary resistance of structured random beams to atmospheric turbulence and their outstanding self-healing ability upon encountering obstacles.<sup>21–24</sup> In particular, the authors of Ref. 24 have demonstrated that there exist structured random beams maintaining their intensity profile structure in the turbulent atmosphere over a distance determined by the turbulence strength. In contrast to fully spatially coherent fields,<sup>25</sup> structured random fields possess a new degree of freedom, the normalized auto-correlation function of the fields at a pair of points across the source, known as the degree of coherence of a source.<sup>26,27</sup> This DoF has been explored to realize high-security optical data storage and retrieval.<sup>28</sup> Moreover, various aspects of optical field correlations at the source, for example, their spatial structure, transverse coherence radius, or classical entanglement,<sup>29</sup> provide access to numerous, untapped, mutually orthogonal DoFs that can be employed for high-capacity, high-fidelity optical communications through complex environments.

In this Letter, we combine structured random light engineering at the source to encode an image into the unique DoFs of such light and deep learning framework at the receiver to propose theoretically and realize experimentally high-fidelity image transmission through a complex environment. In particular, we employ statistically homogeneous, Laguerre–Gaussian correlated sources that produce optical fields with ring correlation structure at the source and ring-like far-field intensity profiles. We demonstrate that such ring-like patterns can be utilized to encode image information. We also show how the source coherence radius can be used as another independent DoF for information encoding. Furthermore, we demonstrate experimentally that supreme resilience of structured random light to atmospheric fluctuations and their excellent ability to self-heal upon encountering obstacles augurs well for the fidelity of image transfer, at least, over short free-space communication links. We reveal the multiplexing capabilities of unique DoFs of random light. For instance, we show how the source coherence radius can be multiplexed with the space position of any beamlet within an array of partially coherent beams carrying image information to the receiver. These multiplexing capabilities demonstrate the potential for significant enhancement of information capacity within our protocol.

Yet another innovation of our protocol is the use of deep learning network capabilities for pattern classification at the decoding stage. In recent years, deep learning has enjoyed immense success in computer science, making it possible to advance data-driven artificial intelligence technologies, such as computer vision,<sup>30</sup> speech recognition,<sup>31</sup> and decision making.<sup>32</sup> Recent applications of deep learning in photonics range from accurate prediction of resonance spectra<sup>33</sup> and inverse design of photonic devices<sup>34</sup> to high-resolution retrieval of orbital angular momentum states<sup>35</sup> and accurate phase prediction for anisotropic digital coding metasurfaces.<sup>36</sup> Although a deep convolutional neural network (CNN), which can be applied to classification tasks,<sup>37</sup> is the most popular, recently proposed residual networks (ResNets), which can scale up to thousands of layers, have demonstrated excellent promise for classification tasks with low training errors.<sup>38</sup> For these reasons, we employ ResNet 34 for image decoding at the receiver end.

The fusion of random light structuring at the transmitter and deep learning image classification at the receiver renders our protocol a promising candidate to realize high-fidelity optical image transmission through a noisy link with a potential to attain high communication channel capacity via tapping into unique crosstalk-free DoFs available to random light sources. As an added bonus, our work will undoubtedly inform further research in the topical field of deep learning network applications to photonics.

Consider a structured random light field propagating along the  $z$  axis. In the space-frequency representation, we can describe the second-order correlations of the fields at a pair of points  $\mathbf{r}_1$  and  $\mathbf{r}_2$  in the transverse plane of the source in terms of a cross-spectral density of the source. We can express the cross-spectral density of any physically realizable statistical source as<sup>39</sup>

$$W_0(\mathbf{r}_1, \mathbf{r}_2) = \int d\mathbf{k} p(\mathbf{k}) H^*(\mathbf{r}_1, \mathbf{k}) H(\mathbf{r}_2, \mathbf{k}). \quad (1)$$

Here,  $H(\mathbf{r}, \mathbf{k})$  is an arbitrary kernel at a temporal frequency  $\omega$  and  $p(\mathbf{k})$  is a non-negative spectral distribution function in the reciprocal  $k$ -space; we will drop any explicit dependence on  $\omega$  hereafter.

Let us now focus on statistically homogeneous light sources for which  $H(\mathbf{r}, \mathbf{k}) = \sqrt{I(\mathbf{r})} e^{i\mathbf{k}\cdot\mathbf{r}}$ , where  $I(\mathbf{r})$  is a source intensity profile.<sup>39</sup> It then follows at once from Eq. (1) that the degree of coherence  $\mu_0(\mathbf{r}_1 - \mathbf{r}_2)$  of such a source, defined as a normalized second-order correlation function  $\mu_0(\mathbf{r}_1, \mathbf{r}_2) = W_0(\mathbf{r}_1, \mathbf{r}_2) / \sqrt{I(\mathbf{r}_1)I(\mathbf{r}_2)}$ ,<sup>25,26</sup> is simply a Fourier transform of  $p(\mathbf{k})$ . Furthermore, the far-field intensity profile of a low-coherence source has the same functional form as  $p(\mathbf{k})$ .<sup>26</sup> Therefore, the spatial structure of source correlations, or equivalently, its spectral density distribution  $p(\mathbf{k})$  can serve as an independent DoF for information encoding. We choose a Laguerre–Gaussian (LG) correlated Schell-model source as a representative example.<sup>40</sup> The spectral density of such a source reads

$$p(\mathbf{k}) \propto (\mathbf{k}^2 \sigma_c^2 / 2)^{|l|} \left[ L_p^{|l|}(\mathbf{k}^2 \sigma_c^2 / 2) \right]^2 e^{-\mathbf{k}^2 \sigma_c^2 / 2}. \quad (2)$$

Here,  $\sigma_c$  is a coherence radius of the source and  $L_p^{|l|}$  stands for an associated Laguerre polynomial of azimuthal  $l$  and radial  $p$  indices, respectively. We can then generate a multitude of LG-correlated sources by varying  $p$  and  $l$ . Furthermore, one can easily verify that a Fourier transform of the spectral density of the LG-correlated source yields yet another LG-like spatial pattern.

We are now in a position to describe our strategy to encode a desired image into an ensemble of light beams generated by an LG-correlated source. We sketch the schematics of our protocol in Fig. 1. We exhibit 4 LG profile patterns, which we refer to as states hereafter, as an illustrative example of image encoding into LG spatial correlations of a source. The source produces an ensemble of LG-correlated beams of spot size  $w = 0.68$  mm and coherence radius  $\sigma_c = 0.1$  mm, propagating from the source (transmitter) to a receiver. The ensemble contains LG states corresponding to four index parameters: LG<sub>10</sub>, LG<sub>20</sub>, LG<sub>12</sub>, and LG<sub>22</sub>. The transmitted information in our protocol is a 16-gray-level (8, 24, 40, 56, 72, 88, 104, 120, 136, 152, 168, 184, 200, 216, 232, and 248) image of Lena, which has  $100 \times 100$  pixel resolution. The gray level of the image is quantified by 2-digit quaternary numbers (00, 01, 02, 03... 32, 33). Here, every quaternary number corresponds to an LG-correlated beam structure (0 is LG<sub>10</sub>, 1 is LG<sub>20</sub>, 2 is LG<sub>12</sub>, and 3 is LG<sub>22</sub>). Therefore, we can encode the gray level of each

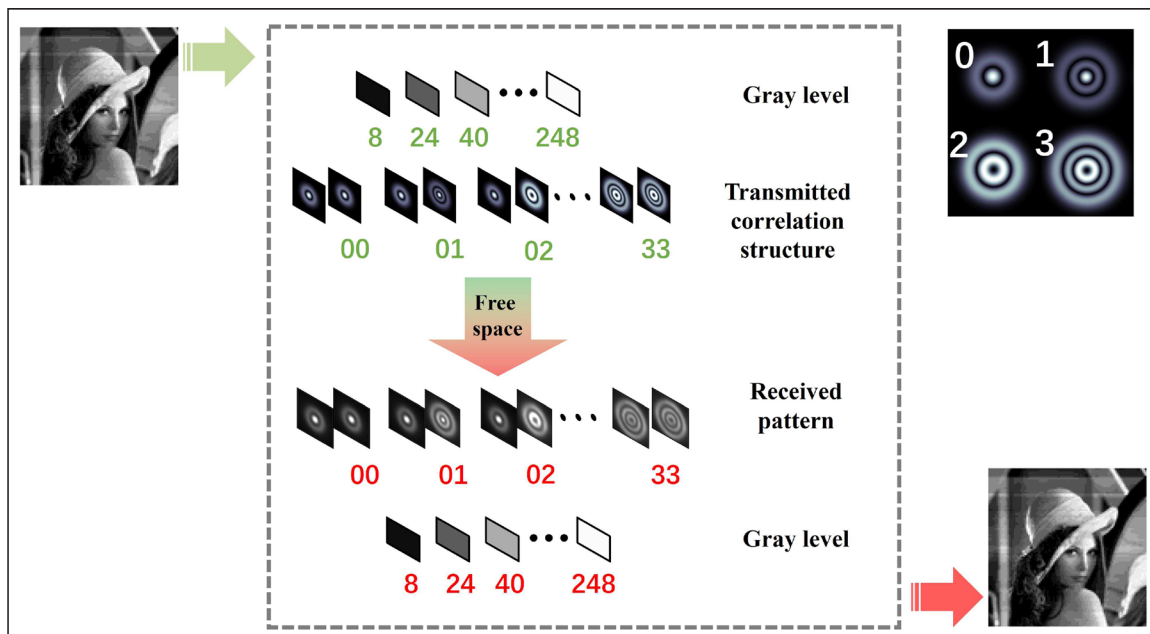


FIG. 1. Schematics of our encoding/decoding protocol with LG-correlated beams.

pixel at the transmitter and store it in 2 LG-correlated beam structures. Next, we transmit the encoded information from the source to the receiver in free space, or realistically through a random medium, with the aid of an ensemble of LG-correlated beams. In the case of free-space propagation, the intensity patterns at the receiver, situated in the far-zone of the source, are proportional to  $p(\mathbf{k})$ , which is evaluated at  $\mathbf{r}$ . Furthermore, we record the intensity patterns of the received beam ensemble with a CCD camera and decode them into a set of quaternary numbers following the encoding rules. Finally, we collect a set of pixels of variable gray level encapsulating the transmitted image.

We employ a deep residual learning ResNet architecture with 34 layers, known as ResNet 34 network. The network is only interested in the image of intensity patterns and these patterns are directly accessible to the computers. First, we order sequentially all members of an LG-correlated beam ensemble recorded by the camera. In the following step, we have the network classify the received images and map them into quaternary numbers for subsequent decoding. Thus, each intensity pattern can be converted into a set of digital numbers by the classifier network as shown in Fig. 2. We display the basic framework of ResNet 34 classifier in the dashed square of Fig. 2 and we discuss the details of the overall structure of the network in Sec. I of the [supplementary material](#), see especially Table S1 and Fig. S1. We now outline how ResNet 34 works in a classifier mode. Inspired by the concept of transfer learning, we use the pre-trained parameters, which have been previously trained and tested on the ImageNet dataset,<sup>41</sup> for initialization. We then fine-tune ResNet 34 with our images to suit a particular classification task. At the outset, we prepare 200 experimental images with labels for each category and combine them into a training dataset. Next, we resize all the training images to  $224 \times 224$  to be served as input to the network. To obtain a robust classifier model, we divide the whole training dataset randomly into three non-overlapping subsets in

proportion 70%, 20%, and 10%, corresponding to the training, validation, and test sets, respectively. Specifically, to avoid any bias caused by class imbalance, we make sure that the number of different class samples is the same in each subset. We utilize the training set to learn the characteristics of the data and develop a model. The validation set is used to adjust the parameters and hyper-parameters of the model during the training process to improve the model performance. The test set should not be used in the training phase and is used to evaluate the performance and robustness of the model on unseen data.<sup>42</sup> Having taken these steps, we have established a robust ResNet 34 network ready to classify images. We then resize the images to be tested and feed them into the established classification network, which realizes decoding in our protocol. Each tested image corresponds to the network output category, with the corresponding quaternary number specifying its gray level. Once the decimal gray value of each pixel is obtained, we can identify the whole image.

We verify our protocol by carrying out proof-of-principle image transmission with an experimental setup sketched in Fig. 3(a). First, we produce a fully coherent Gaussian beam with the help of a continuous-wave-diode-pumped laser with the carrier wavelength  $\lambda_0 = 532$  nm and transmit the beam through a neutral density filter (NDF). After having been expanded and collimated by a beam expander (BE) comprised of two lenses of different focal length,  $L_1$  and  $L_2$ , the beam is reflected by a spatial light modulator (SLM), which displays a hologram dataset of LG patterns encapsulating the encoded information. Thereby, the generated LG beams are focused by a lens  $L_3$  ( $f = 250$  mm) and projected onto a rotating ground glass disk (RGGD), which we place in the front focal plane of a collimating lens  $L_4$ . Next, an LG-correlated beam emerges past  $L_4$  ( $f = 150$  mm) and a Gaussian amplitude Filter (GAF) and we encode the transmitted information into its spatial correlation

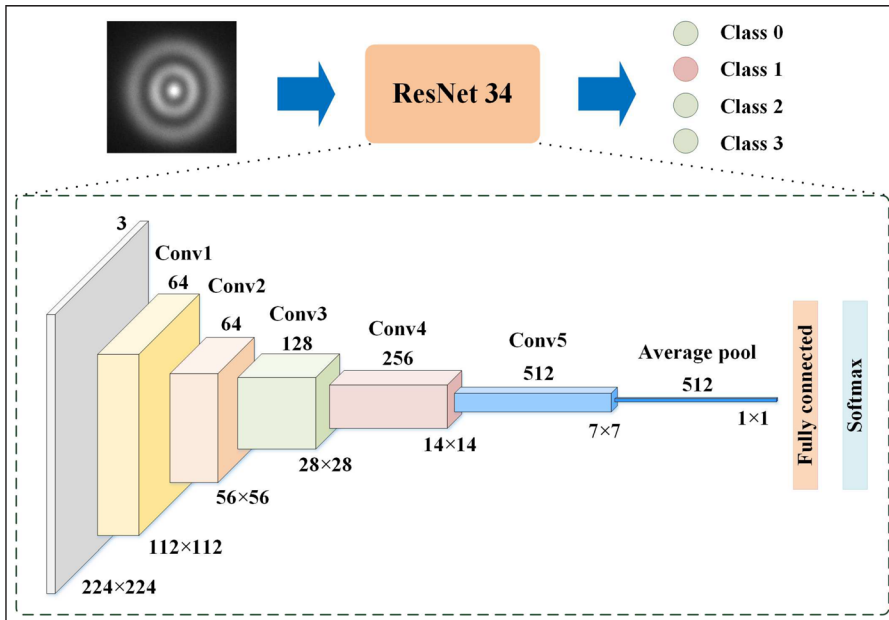


FIG. 2. Decoding process and the architecture of ResNet 34 classifier.

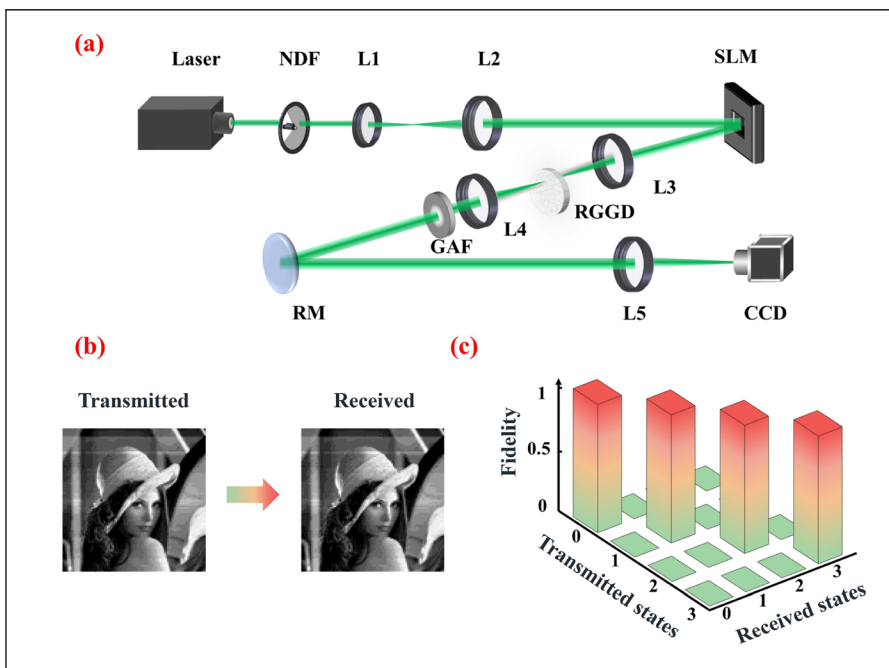


FIG. 3. Experimental verification of our protocol. (a) Experimental setup. NDF: neutral density filter; L: thin lens; RGGD: rotating ground glass disk; GAF: Gaussian amplitude filter; SLM: spatial light modulator; RM: reflected mirror; and CCD: charge coupled device. (b) Qualitative juxtaposition of transmitted and received images. (c) Quantitative measure of the state detection fidelity as a conditional probability  $P_{s_r|s_t}$  of finding a transmitted state  $s_t$  in state  $s_r$ , where  $s_r(s_t)$  is represented in the quaternary basis (0, 1, 2, 3).

structure. Having propagated a 1.92 m stretch of free space, the beam is focused onto a charge coupled device (CCD) camera by a lens  $L_5$  ( $f=150$  mm). The camera serves as a receiver recording the intensity patterns of an LG-correlated beam ensemble.

We contrast the transmitted and received images of Lena in Fig. 3(b). We can readily infer from the figure that there is excellent qualitative resemblance between the transmitted and received images attesting to the viability of our protocol. We then quantify the fidelity

of each state in terms of a conditional probability  $P_{s_r|s_t}$  of finding a transmitted state  $s_t$  in state  $s_r$ , and the total signal error rate can also be evaluated as  $\sum_{s_r \neq s_t} P(s_r|s_t)P(s_t)$ .<sup>17</sup> We summarize the results in Fig. 3(c). The multitude of  $100 \times 100 \times 2 = 20\,000$  received states are recognized by the ResNet 34 network, and the attained fidelity of the image transfer, evaluated as a fraction of correctly received states vs the total number of transmitted states, exceeds 99.99%. In other words, the total average signal error rate is less than  $10^{-4}$ .



We now elucidate the role of noise due to either atmospheric turbulence or opaque obstacle scattering on image transmission quality within the framework of our protocol. There has been a growing body of evidence, see, for instance, Ref. 21 for a review that decreasing spatial coherence of a light source enhances the resilience of the beams generated by such a partially coherent source to random perturbations in a complex environment. To verify this conjecture, we record the intensity patterns of LG-correlated beams propagating through a random medium mimicking atmospheric turbulence and compare them with those of fully coherent LG beams propagating through the same medium. We use optical diffusers (ODs) to simulate turbulence, see the [supplementary material](#) for further information. We can infer from Fig. 4 that fully coherent LG beams are more distorted than their partially coherent cousins. This observation implies that image transmission through random medium and recovery of fully coherent LG beams is much more complicated and time-consuming as well as far less accurate than that with LG-correlated beams. Moreover, the situation exacerbates as the turbulence strength increases. We can model stronger turbulence with two ODs as opposed to weaker turbulence, which can be modeled with just a single diffuser. By comparing the corresponding panels of Fig. 4, we observe that the advantage of reducing source coherence of the beam augments for stronger turbulence: We clearly distinguish a ring structure of the LG-correlated beam in stronger turbulence, while the intensity profile of a fully coherent LG beam swiftly turns into essentially a random speckle pattern.

To test our protocol in the more adverse situation, we repeat all protocol steps, except we include two ODs to model stronger turbulence as a propagation milieu. We transmit a 16-gray-level Lena image of  $80 \times 80$  pixel resolution. We present a schematic of the experimental setup in Fig. S2 of the [supplementary material](#). The received intensity patterns remain distinguishable and can be decoded directly by ResNet 34, thereby avoiding redundant processing and helping save

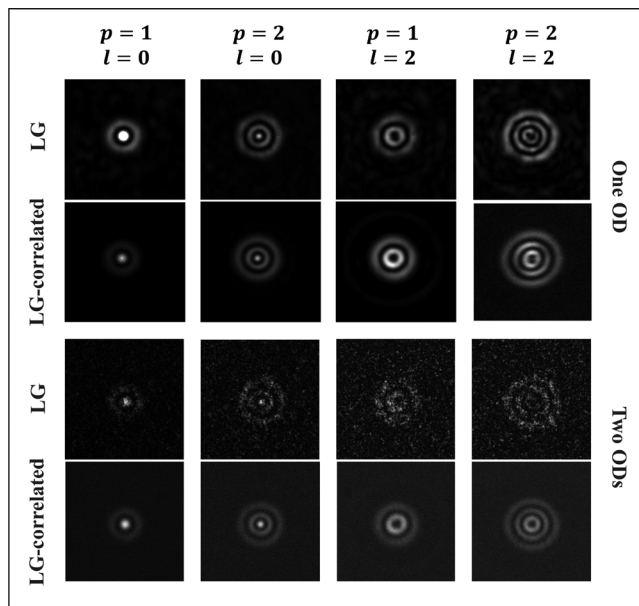


**FIG. 4.** Recorded intensity profiles of LG-correlated vs fully coherent LG beams transmitted through either a single or two optical diffusers.

time. Our results show good tolerance of the protocol to medium turbulence and yield the fidelity of image retrieval of over 99.99%, corresponding to a total signal error rate lower than  $10^{-4}$ , see Fig. S7(a).

By the same token, random beams of sufficiently low coherence are known to self-heal upon encountering discrete obstacles such as suspended particles in free space.<sup>22</sup> In Fig. S3 of the [supplementary material](#), we provide experimental evidence of LG-correlated beam self-healing capabilities and then repeat the protocol for image transmission and realize a fidelity of over 99.99%, see also Fig. S7(b). We remark that the extremely high fidelity of image transmission in free-space and turbulent or colloidal particle medium is achieved thanks to the superb job that a deep learning network, such as ResNet 34, does to faithfully decode images.

An alternative strategy involves information encoding into transverse coherence radius of the light source, which can be viewed as another independent degree of freedom for free-space optical communications. The details of this protocol, which are quite similar to those of the previously described one, can be found in Sec. IV of the [supplementary material](#). As is evidenced by Fig. S7(c), the received image bears excellent resemblance to the transmitted one, attesting to the viability of our protocol.

The two protocols that we have described thus far involve two independent DoFs for free-space optical communications: the spatial structure of the source degree of coherence and the coherence radius of the source. Each of these DoFs can be multiplexed with other optical field characteristics, such as spatial, polarization, and spectral (wavelength) DoFs, to boost the communication capacity of the protocol.

In the [supplementary material](#), we illustrate multiplexing the coherence radius and spatial location of a beamlet within a source array to demonstrate but one among multiple perspectives. The operation is introduced in Sec. V of the [supplementary material](#). The results shown in Fig. S8 imply a transmission fidelity of 99.99% and total signal error rate of  $10^{-4}$ .

We have theoretically proposed and experimentally implemented a free-space optical communication protocol enabling high-fidelity transfer of a desired information through, in general, a noisy communication channel. The key innovation of the proposed protocol is the fusion of random source structuring at the transmitter end and the employment of a deep learning network at the receiver end. The structuring of random source makes it possible to tap into multiple hitherto unexplored DoFs for image encoding, including the two that have been explicitly demonstrated to yield high-fidelity information transfer: the coherence structure of the source and the source coherence radius. Furthermore, we also demonstrated the capability of our protocol for multiple DoF multiplexing to greatly enhance its communication capacity. In addition, using structured random light ensures resilience of the transmitted image to channel noise such as medium turbulence or the presence of solid obstacles in the light propagation path. The high-fidelity of our protocol is achieved due to two factors. First, the structured random light is robust against random perturbations in the medium. Second and most important, the deep learning network, which we employ for information decoding, enables extremely accurate image recognition in a time efficient manner, compared to other proposed imaging protocols.<sup>28</sup>

See the [supplementary material](#) for the details on experimental verification of our protocol in complex environment, image

transmission utilizing source coherence radius, multiplexing the coherence radius and spatial location, comparison between transmitted and received images, and fidelity evaluation.

This work was supported by the National Key Research and Development Program of China (Nos. 2022YFA1404800 and 2019YFA0705000), the National Natural Science Foundation of China (Nos. 12192254, 92250304, and 12274268), the China Scholarship Council (202108370219), and the Natural Sciences and Engineering Research Council of Canada (RGPIN-2018-05497).

## AUTHOR DECLARATIONS

### Conflict of Interest

The authors have no conflicts to disclose.

### Author Contributions

**Xiaofei Li:** Data curation (equal); Formal analysis (equal); Methodology (equal); Writing – original draft (equal). **Yu Wang:** Writing – original draft (equal). **Xin Liu:** Formal analysis (equal). **Yuan Ma:** Formal analysis (equal). **Yangjian Cai:** Funding acquisition (equal); Supervision (equal). **Sergey A. Ponomarenko:** Funding acquisition (equal); Supervision (equal); Writing – review & editing (equal). **Xianlong Liu:** Funding acquisition (equal); Writing – review & editing (equal).

### DATA AVAILABILITY

The data that support the findings of this study are available from the corresponding author upon reasonable request.

### REFERENCES

- Y. Okawachi, B. Y. Kim, M. Lipson, and A. L. Gaeta, “Chip-scale frequency combs for data communications in computing systems,” *Optica* **10**(8), 977–995 (2023).
- I. Khader, H. Bergeron, L. C. Sinclair, W. C. Swann, N. R. Newbury, and J. D. Deschênes, “Time synchronization over a free-space optical communication channel,” *Optica* **5**(12), 1542–1548 (2018).
- K. Zou, K. Pang, H. Song, J. Fan, Z. Zhao, H. Song, R. Zhang, H. Zhou, A. Minoofar, C. Liu, X. Su, N. Hu, A. McClung, M. Torfeh, A. Arbabi, M. Tur, and A. E. Willner, “High-capacity free-space optical communications using wavelength- and mode-division-multiplexing in the mid-infrared region,” *Nat. Commun.* **13**, 7662 (2022).
- Z. Huang, X. Hu, Q. Li, X. Jin, B. Xu, D. Wang, X. Liu, T. Zhang, Z. Zhang, G. Chen, C. Li, and D. Li, “Phase-shifted quadrature-phase demodulation based on a multi-longitudinal mode laser self-mixing sensor for displacement measurement,” *Measurement* **206**, 112323 (2023).
- B. Stern, H. Chen, K. Kim, and N. K. Fontaine, “Large dispersion silicon Bragg grating for full-field 40-GBd QPSK phase retrieval receiver,” *J. Lightwave Technol.* **40**(22), 7358–7363 (2022).
- Z. Duan, H. Chen, and X. Lin, “Optical multi-task learning using multi-wavelength diffractive deep neural networks,” *Nanophotonics* **12**(5), 893–903 (2023).
- C. Huang, D. Wang, W. Zhang, B. Wang, A. N. Tait, T. F. de Lima, B. J. Shastri, and P. R. Prucnal, “High-capacity space-division multiplexing communications with silicon photonic blind source separation,” *J. Lightwave Technol.* **40**(6), 1617–1632 (2022).
- S. A. Derevyanko and J. E. Prilepsky, “Channel model for the dual-polarization b-modulated nonlinear frequency-division multiplexing optical transmission systems,” *Opt. Express* **31**(12), 19686–19702 (2023).
- A. E. Willner and C. Liu, “Perspective on using multiple orbital-angular-momentum beams for enhanced capacity in free-space optical communication links,” *Nanophotonics* **10**(1), 225–233 (2020).
- J. Wang, J. Liu, S. Li, Y. Zhao, J. Du, and L. Zhu, “Orbital angular momentum and beyond in free space optical communications,” *Nanophotonics* **11**(4), 645–646 (2022).
- J. Li, Q. Yang, X. Dai, C. Lim, and A. Nirmalathas, “Joint beam-and-probabilistic shaping scheme based on orbital angular momentum mode for indoor optical wireless communications,” *J. Lightwave Technol.* **41**(20), 6488–6495 (2023).
- H. Cao, A. P. Mosk, and S. Rotter, “Shaping the propagation of light in complex media,” *Nat. Phys.* **18**, 994–1007 (2022).
- Z. Xu, G. Xu, and Z. Zheng, “BER and channel capacity performance of an FSO communication system over atmospheric turbulence with different types of noise,” *Sensors* **21**(10), 3454 (2021).
- R. Zhang, N. Hu, H. Zhou, K. Zou, X. Su, Y. Zhou, H. Song, K. Pang, H. Song, A. Minoofar, Z. Zhao, C. Liu, K. Manukyan, A. Almaiman, B. Lynn, R. W. Boyd, M. Tur, and A. E. Willner, “Turbulence-resilient pilot-assisted self-coherent free-space optical communications using automatic optoelectronic mixing of many states,” *Nat. Photonics* **15**, 743–750 (2021).
- M. Ghalaii and S. Pirandola, “Quantum communications in a moderate-to-strong turbulent space,” *Commun. Phys.* **5**, 38 (2022).
- H. Zhou, X. Su, Y. Duan, H. Song, K. Zou, R. Zhang, H. Song, N. Hu, M. Tur, and A. E. Willner, “Atmospheric turbulence strength distribution along a propagation path probed by longitudinally structured optical beams,” *Nat. Commun.* **14**, 4701 (2023).
- Z. Zhu, M. Janasik, A. Fyffe, D. Hay, Y. Zhou, B. Kantor, T. Winder, R. W. Boyd, G. Leuchs, and Z. Shi, “Compensation-free high-dimensional free-space optical communication using turbulence-resilient vector beams,” *Nat. Commun.* **12**(1), 1666 (2021).
- L. Gong, Q. Zhao, H. Zhang, X. Hu, K. Huang, J. Yang, and Y. Li, “Optical orbital-angular-momentum-multiplexed data transmission under high scattering,” *Light* **8**(1), 27 (2019).
- S. Li and J. Wang, “Adaptive free-space optical communications through turbulence using self-healing Bessel beams,” *Sci. Rep.* **7**(1), 43233 (2017).
- Y. Shen, S. Pidishety, I. Nape, and A. Dudley, “Self-healing of structured light: A review,” *J. Opt.* **24**(10), 103001 (2022).
- F. Wang, X. Liu, and Y. Cai, “Propagation of partially coherent beam in turbulent atmosphere: A review,” *Prog. Electromagn. Res.* **150**, 123–143 (2015).
- F. Wang, Y. Chen, X. Liu, Y. Cai, and S. A. Ponomarenko, “Self-reconstruction of partially coherent light beams scattered by opaque obstacles,” *Opt. Express* **24**, 23735–23746 (2016).
- Z. Xu, X. Liu, Y. Chen, F. Wang, L. Liu, Y. E. Monfared, S. A. Ponomarenko, Y. Cai, and C. Liang, “Self-healing properties of Hermite-Gaussian correlated Schell-model beams,” *Opt. Express* **28**, 2828–2837 (2020).
- Z. Xu, X. Liu, Y. Cai, S. A. Ponomarenko, and C. Liang, “Structurally stable beams in the turbulent atmosphere: Dark and antidark beams on incoherent background [Invited],” *J. Opt. Soc. Am. A* **39**(12), C51–C57 (2022).
- S. A. Ponomarenko and E. Wolf, “The spectral degree of coherence of fully spatially coherent electromagnetic beams,” *Opt. Commun.* **227**, 73–74 (2003).
- L. Mandel and E. Wolf, *Optical Coherence and Quantum Optics* (Cambridge University Press, Cambridge, 1995).
- S. A. Ponomarenko and E. Wolf, “Coherence properties of light in Young’s interference pattern formed with partially coherent light,” *Opt. Commun.* **170**, 1–8 (1999).
- X. Liu, S. A. Ponomarenko, F. Wang, Y. Cai, and C. Liang, “Incoherent mode division multiplexing for high-security information encryption,” *arXiv:2304.06455* (2023).
- S. A. Ponomarenko, “Twist phase and classical entanglement of partially coherent light,” *Opt. Lett.* **46**, 5958–5961 (2021).
- W. Liu, D. Ma, Z. Li, H. Cheng, D.-Y. Choi, J. Tian, and S. Chen, “Aberration-corrected three-dimensional positioning with a single-shot metalens array,” *Optica* **7**, 1706 (2020).
- G. Hinton, L. Deng, D. Yu, G. E. Dahl, A. Mohamed, N. Jaitly, A. Senior, V. Vanhoucke, P. Nguyen, T. N. Sainath, and B. Kingsbury, “Deep neural networks for acoustic modeling in speech recognition: The shared views of four research groups,” *IEEE Signal Process. Mag.* **29**, 82–97 (2012).
- D. Silver, A. Huang, C. J. Maddison, A. Guez, L. Sifre, G. Van Den Driessche, J. Schrittwieser, I. Antonoglou, V. Panneershelvam, M. Lanctot, S. Dieleman, D. Grewe, J. Nham, N. Kalchbrenner, I. Sutskever, T. Lillicrap, M. Leach, K.

- Kavukcuoglu, T. Graepel, and D. Hassabis, "Mastering the game of Go with deep neural networks and tree search," *Nature* **529**, 484–489 (2016).
- <sup>33</sup>W. Ma, F. Cheng, and Y. Liu, "Deep-learning-enabled on-demand design of chiral metamaterials," *ACS Nano* **12**, 6326 (2018).
- <sup>34</sup>Z. Liu, D. Zhu, S. P. Rodrigues, K.-T. Lee, and W. Cai, "Generative model for the inverse design of metasurfaces," *Nano Lett.* **18**, 6570 (2018).
- <sup>35</sup>Z. Liu, S. Yan, H. Liu, and X. Chen, "Superhigh-resolution recognition of optical vortex states assisted by a deep-learning method," *Phys. Rev. Lett.* **123**, 183902 (2019).
- <sup>36</sup>Q. Zhang, C. Liu, X. Wan, L. Zhang, S. Liu, Y. Yang, and T. J. Cui, "Machine-learning designs of anisotropic digital coding metasurfaces," *Adv. Theor. Simul.* **2**, 1800132 (2019).
- <sup>37</sup>A. Krizhevsky, I. Sutskever, and G. E. Hinton, "ImageNet classification with deep convolutional neural networks," in 25th International Conference on Neural Information Processing Systems (NIPS, 2012), Vol. 1, p. 1097.
- <sup>38</sup>K. He, X. Zhang, S. Ren, and J. Sun, "Deep residual learning for image recognition," in *Proceedings of the IEEE Conference on Computer Vision and Pattern Recognition (CVPR)* (IEEE, 2016), pp. 770–778.
- <sup>39</sup>F. Gori and M. Santarsiero, "Devising genuine spatial correlation functions," *Opt. Lett.* **32**(24), 3531–3533 (2007).
- <sup>40</sup>C. Liang, R. Khosravi, X. Liang, B. Kacerovská, and Y. E. Monfared, "Standard and elegant higher-order Laguerre-Gaussian correlated Schell-model beams," *J. Opt.* **21**(8), 085607 (2019).
- <sup>41</sup>O. Russakovsky, J. Deng, H. Su, J. Krause, S. Satheesh, S. Ma, Z. Huang, A. Karpathy, A. Khosla, M. Bernstein, A. C. Berg, and L. Fei-Fei, "ImageNet large scale visual recognition challenge," *Int. J. Comput. Vis.* **115**, 211–252 (2015).
- <sup>42</sup>Y. Chen, S. Zhang, and R. Song, "Scoring your prediction on unseen data," in *Proceedings of the IEEE Conference on Computer Vision and Pattern Recognition (CVPR)* (IEEE, 2023), pp. 3278–3287.